Rate Constants in Two Dimensions of Electron Transfer between Pyruvate Oxidase, a Membrane Enzyme, and Ubiquinone (Coenzyme Q_8), Its Water-Insoluble Electron Carrier

Damien Marchal,[‡] Jacques Pantigny,[‡] Jean Marc Laval,[‡] Jacques Moiroux,[§] and Christian Bourdillon*[,‡]

Laboratoire de Technologie Enzymatique, Unité associée au CNRS No. 6022, Université de Technologie de Compiègne, B.P. 20529, 60205 Compiègne Cedex, France, Laboratoire d'Electrochimie Moléculaire, Unité associée au CNRS No. 7591, Université Paris, 7-Denis Diderot, 75251 Paris Cedex 05, France

Received October 4, 2000

ABSTRACT: The functionality of the membrane-bound, ubiquinone-dependent pyruvate oxidase from the respiratory chain of *Escherichia coli* was reconstituted with a supported lipidic structure. The artificial structure was especially designed to allow the electrochemical control of the quinone pool through the lateral mobility of the ubiquinone (Q_8) molecules. The kinetic coupling of the enzyme bound to the lipid structure with the quinone pool was ensured by the regeneration of the oxidized form of ubiquinone at the electrochemical interface. Such an experimental approach enabled us to carry out an unprecedented determination of the kinetic parameters controlling the reaction between the enzyme bound and the electron carrier under conditions taking rigorously into account the fact that the freedom of motion is restricted to two dimensions. The kinetic constants we found show that the activated enzyme can be efficiently regulated by the oxidation level of the quinone pool in natural membranes.

In electron transfer chains, many enzyme complexes utilize membrane-bound electron carriers such as water-insoluble quinones, which are specifically confined to the hydrophobic part of the membrane. Kinetics of such enzymes has been considered within the framework of the random collision model of electron transport which has been well documented (*1*, *2*). Experimental approaches and interpretations must take into account the fact that the membrane enzyme molecules are fed by molecules diffusing either in three or two dimensions.

To determine experimentally the kinetic parameters involved in these complex systems, numerous structural and analytical difficulties must be overcome (*2*). First, membrane enzymes catalyze reactions in a highly organized environment. In vitro kinetic experiments require the reconstitution of enzymes into artificial structures made of self-assembled lipids, most frequently proteoliposomes or supported plane bilayers. Second, the electron carriers move laterally within the bilayer, and the corresponding dynamic behavior must be analyzed concomitantly with the catalysis to characterize correctly the kinetics of the system. Third, the reaction velocity is sensitive to the surface concentration of the electron carrier which moves only in two dimensions. Consequently, the steady-state rate equations must be modified to take into account a reduction in dimensionality since the redox carrier diffuses only into small specific regions of the total reaction volume (*3*, *4*). For example, a second-order rate constant is expressed in $cm^2\ mol^{-1}\ s^{-1}$ instead of $cm^3\ mol^{-1}\ s^{-1}$. To overcome the difficulty, artificial water-soluble mediators were very often substituted for the natural hydrophobic quinones, and the kinetics were monitored spectrophotometrically, for example, in suspensions of proteoliposomes. By doing so, the two-dimension nature of the electron transport is lost and the electron transfer can be controlled by nonphysiological parameters since the approach of the hydrophilic electron carrier to the enzymatic site is essentially different.

We propose in this work a new approach for the experimental determination of the two-dimension kinetic parameters controlling the kinetics of a membrane enzyme. As the phenomena of interest are fundamentally heterogeneous, we used cyclic voltammetry that deals basically with heterogeneous concepts to monitor the catalysis. Moreover, the use of an electrochemical method is especially convenient for the study of electron carriers such as ubiquinones which are electrochemically active.

We developed recently a "microporous electrode", a special type of electrode that allows the direct electrochemistry of water-insoluble isoprenic quinones incorporated in a model of bilayer (*5*−*8*). Technically, the structure produced by electrochemical corrosion of aluminum is an array, surprisingly regular, of cylindrical pores (Figure 1) (*9*). The pores of about 100 nm diameter are oriented perpendicularly to the electrode (a gold interface formed by vapor deposition under vacuum). The porous structure is the template for the construction of a bilayer resulting from the adsorption of vesicles onto a preformed alkyl monolayer. The quinone molecules are incorporated through this self-assembly procedure. Such artificial bilayers formed on alkylated layers

* To whom correspondence should be addressed: Christian Bourdillon, Laboratoire de Technologie Enzymatique, Université de Technologie de Compiègne, B. P. 20529, 60205 Compiègne Cedex, France. E-mail: Christian.Bourdillon@utc.fr. Telephone: (33) 3 44 23 44 05. Fax: (33) 3 44 20 39 10.

[‡] Université de Technologie de Compiègne.

[§] Université Paris.

10.1021/bi002325y CCC: $20.00
Published on Web 01/11/2001

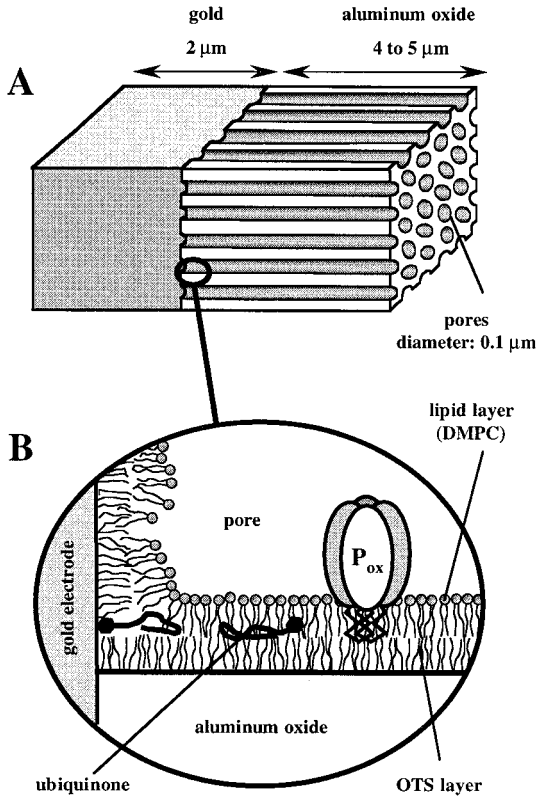

FIGURE 1: (A) Structure of the microporous electrode made of a porous aluminum oxide film attached to a gold electrode. The porous oxide is the template of the self-assembled lipid layer. For a 3-mm diameter electrode, the effective surface area of the layer is ca. 5 cm^2. (B) Enlarged schematic view of a pore bottom at the level of the bilayer/gold interface. The ubiquinone molecules are laterally mobile along the pore wall and reach the electrode at this level. Peripheral enzymes such as pyruvate oxidase can be anchored in the lipid layer along the pore.

are still far from true biological membranes, but it has been demonstrated that some physicochemical properties are correctly mimicked (*10*; recent review in ref *11*). For example, the upper lipid layer behaves as a "liquid like" phase, and the measured lateral diffusion coefficient of DMPC[1] of $(5 \pm 1) \times 10^{-8}$ cm^2 s^{-1} (30 °C) (*7*) lies in the range of data found for membrane model systems (*12*). Ubiquinone or plastoquinone molecules bearing isoprenic chains of various lengths were incorporated at a physiological level (0.5 to 2 mol %), and their lateral mobility was ascertained by the dependence of their diffusion coefficient on the isoprenic length (*7*).

The main disadvantage of the above-described hemi-bilayer strategy for the assembly of supported biomembrane is the impossibility to incorporate transmembrane proteins. Pending the development of more realistic models that are the subject of intense current research (see recent reviews in refs *13* and *14*) and making profit of the fact that one side of the hemi-bilayer exhibits normal properties, we studied in a first approach the behavior of a peripheral enzyme that exchanges electrons with ubiquinone. We chose pyruvate oxidase (POx) from *Escherichia coli* (EC 1.2.2.2.) since it can be purified from the cytoplasmic membrane and reincorporated into proteoliposomes without using detergents, a decisive advantage for our model. POx is a flavoprotein from the aerobic respiratory chain of *E. coli* that oxidizes pyruvate to produce acetic acid and carbon dioxide and reduces ubiquinone (Q_8) in the cytoplasmic membrane (*15*). In the absence of substrate and cofactor (thiamin pyrophosphate TPP) POx is a water-soluble protein which can be purified without the use of detergents (*16*, *17*). However, in the presence of substrate and TPP, the reduced enzyme undergoes a conformational change exposing a membrane binding site (*16*, *18*). Under the latter conditions, the POx structure is tetrameric, the enzyme is activated by phospholipids and manifests the catalytic properties of a true peripheral enzyme (*19*, *20*).

In the present work, after self-assembly of the different components (lipids, ubiquinone, POx) in the mimetic structure, the electrochemical reaction was used to control and monitor the surface concentrations of both the oxidized and reduced forms of the quinone pool within the bilayer. The kinetic coupling of the electrochemical reaction with the bilayer bound enzyme catalyzed reaction, through the diffusion of the ubiquinone/ubiquinol molecules within the bilayer, enabled us to characterize quantitatively the complete set of relevant kinetics parameters. Such a new approach takes into account, both experimentally and theoretically, the two-dimension nature of the system.

EXPERIMENTAL PROCEDURES

Materials. Thiamine pyrophosphate, sodium pyruvate, L-α-dimyristoylphosphatidylcholine (synthetic >99% pure) were purchased from Sigma (St Quentin Fallavier, France). Ubiquinone (Q_8) was a generous gift from EISAI Company LTD, Tokyo. Octadecyltrichlorosilane, (Aldrich, Strasbourg, France) was vacuum-distilled before use. Hexadecane (Aldrich) was dried over desiccated molecular sieves. Octadecyl mercaptan was from Aldrich. Aluminum foil, 1 mm thick (Al 99.95%), was from Merck (Darmstadt, Germany). Organic solvents were HPLC-grade. Water with a typical resistivity of 18 MΩ was produced from Milli-Q purification system (Millipore, Les Ulis, France). All other chemicals were reagent grade.

E. coli pyruvate oxidase was from the mutant strain YYC 458, generously given by the University of Illinois (L. P. Hager laboratory). It was purified according to the method described by the University of Illinois group (*16*, *17*) after slight modification (*21*). After purification and pooling in a phosphate buffer plus 25% glycerol (v/v) for storage at −20 °C, the final POx sample exhibited a protein concentration (Bradford) of 1.25 mg/cm^3 and a catalytic activity of 270 μmol of ferricyanide min^{-1} mg^{-1} of flavoprotein subunit using the standard ferricyanide assay at 25 °C (*15*). The flavin absorbance at 438 nm ($\epsilon = 14900$ M^{-1} cm^{-1} from ref *22*) indicated that some FAD was lost during the purification procedure since about 45% of the protein in the POx sample was not the intact flavoprotein.

Preparation of the Microporous Electrodes. The modified electrodes were prepared with very thin porous aluminum oxide films (a few micrometers) produced in the laboratory. The procedure was first described by Miller and Majda (*23*) and modified by Parpaleix et al. (*24*). Briefly, aluminum

[1] DMPC, dimyristoyl phosphatidylcholine; OTS, octadecyl trichloro silane; OM, octadecyl mercaptan; OG, octyl D-glucoside; POx, pyruvate oxidase from *E. coli* (EC 1.2.2.2); SCE, saturated calomel electrode; SPR, surface plasmon resonance; TPP, thiamine pyrophosphate; Q_1, Q_8, Q_{10}, ubiquinones molecules with one, eight, or 10 isoprenoid monomers; Q_8H_2, ubiquinol.

oxide films were generated by anodization of aluminum foils. The separation of the oxide film from the aluminum substrate and the removal of the barrier layer were performed according to ref *24*. The thickness (*l*) of these films was between 4 and 5 μm and was routinely measured by scanning electron microscopy with an uncertainty of ±10%. After rinsing in water and drying, the oxide films were alkylated into a freshly prepared OTS solution in hexadecane (1%, v/v). Following a 10 min self-assembly, they were rinsed extensively with toluene and used immediately. They were transferred into a vacuum deposition apparatus (Edwards model E306A) where they were coated with ca. 2-μm-thick gold films. Finally, the gold-coated oxide films were mounted on the tip of a glass tube (3 mm in diameter), using conductive silver glue for electrical contact. The actual surface area of the pores was deduced from scanning electron microphotographs at a magnification of 20000×. Taking into account the pores geometry and the geometrical surface area of the electrode tip (0.07 cm^2), the bilayer surface area was 4.7 ± 0.9 cm^2 for a 4.5-μm-thick oxide film.

The self-assembly of OM on the remaining bare surface of gold brings about a substantial decrease in the level of the microporous electrode background current (*7*). The electrodes were dipped for 3 min in a 1 mM solution of OM in ethanol/water (4/1, v/v). Before use the electrodes were rinsed with ethanol and toluene to remove all unbound OM molecules, then with methanol and, finally, phosphate buffer.

Supported Monolayer Assemblies on Microporous Electrode. Mixed phospholipid-Q_8 vesicles were prepared from dried lipids as follows: the chloroform solution of DMPC and Q_8 in the required ratio was evaporated under nitrogen flow and dried under vacuum for 1 h. The film was resuspended from the walls of a glass tube by vigorous vortexing in 5 mL of water. This solution was sonicated to clarity, 4 times for 3 min each, with a Branson model 250 sonicator (Danbury, CT) set at 60 W power, the temperature being maintained between 40 and 50 °C, with a cold bath in case of need. The solution was cleaned of titanium particles by centrifugation at 3000*g*. For the homogenization of the vesicles size, the solution was extruded 25 times through a 50-nm polycarbonate filter in an Avestin Lipofast Basic extrusion apparatus. The SUV stock solution (about 10 mM in DMPC) was used during the day.

Direct fusion of vesicles on the flat alkylated surfaces (HPA sensor chips from Pharmacia) or on the inner surfaces of OTS-treated microporous electrodes followed procedures as similar as possible (for the sensor chips procedure, see below). For the microporous electrodes, they were first wetted with methanol or in a 50 mM OG solution and rinsed with water in three different baths. The electrodes were then transferred and incubated for 30 min in the vesicles solution (0.7 mM DMPC) for adsorption and fusion at 30 °C. Before use, the microporous electrodes were rinsed with 1 mM NaOH and water for 10 min to remove the adsorbed vesicles.

It is worth emphasizing that repeated dipping of the electrode in the various solutions did not wash out the lipid layer. In contrast with the observed loss of the layer deposited on a planar surface (*9*), the special geometry of the microporous template protects the structure when the tip of the electrode crosses the air/water interface. The final loading of the POx molecules was thus performed by simple dipping of the electrode in the protein solution.

Surface Plasmon Resonance Analysis. The SPR instrument was a Biacore X (Biacore, Sweden) used with HPA sensor chips (Biacore) which consisted of an OM self-assembled monolayer on a flat gold surface. The HPA sensor chips were cleaned by a 15-min injection of 50 mM OG solutions at a flow rate of 5 μL/min. Then the fusion of the vesicles on the OM layer was carried out at a flow rate of 2 μL/min for 20 min. The lipid layer was washed three times, each during 5 min, at a flow rate of 10 μL/min with 10 mM NaOH to remove the intact vesicles. After this rinsing, the SPR signal was stable and the resulting SPR signal of a fused monolayer was 2000 RU ± 200 RU. POx loading on the supported monolayer and rinsing with the pyruvate solution were carried out at a flow rate of 2 μL/min.

Electrochemical Measurements. An anaerobic electrochemical cell was fitted with three electrodes: a working microporous electrode, a platinum foil auxiliary electrode, and a KCl saturated aqueous calomel reference electrode (SCE = 0.238 V vs the normal hydrogen electrode at 35 °C) to which all potentials are referred. Gentle bubbling of argon or nitrogen reduced the partial pressure of oxygen in the main compartment. The temperature was controlled at 35 °C by water circulation in the outer compartment of the water jacketed cell.

A PAR model 273 potentiostat controlled by a PC computer and a model 270 software package (EG&G Princeton Applied Research, Princeton, NJ) or a Voltalab 32 controlled by a PC computer and a Voltamaster software package (Tacussel, Radiometer Analytical, Villeurbanne, France) were used indifferently for cyclic voltammetry.

RESULTS AND DISCUSSION

Catalytic Coupling in Two Dimensions. It has been previously shown that the microporous alkylated electrodes used in this work are convenient templates for the fusion of lipid vesicles (*5*−*8*). The main physicochemical characteristics of the supported layer are as follows: (i) the surface concentration of the DMPC monolayer is (250 ± 50) × 10^{-12} mol cm^{-2}, (ii) the fusion of vesicles containing a physiological molar fraction of isoprenic quinones (below 2 mol %) leads to the quantitative incorporation of the water-insoluble quinone (*6*), (iii) the upper layer behaves like a "liquid like" phase at 35 °C, (iv) the lateral diffusion coefficients of the Q_8 molecules are found to be 3.8 × 10^{-8} cm^2 s^{-1} at this temperature.

An important advantage of the microporous electrode technology is the possibility of controlling and monitoring the quinone pool directly in the supported layer (*5*−*7*). For example, the thermodynamics of the isoprenic quinones and the dynamics of the electrochemical process at the gold/bilayer interface coupled with the two-dimension diffusion within the lipid bilayer were characterized by means of cyclic voltammetry (*8*). The time dependence of the distribution of the surface concentrations of the oxidized or reduced forms of the ubiquinone within the bilayer was thus known. As compared with the classical measurement of the quinone redox states by dual-wavelength spectrophotometry, this heterogeneous approach offers attractive new possibilities for the study of membrane enzymes.

Figure 2 shows the voltammetric behavior of the quinone pool before and after the assembly of pyruvate oxidase in

the microporous electrode. Ubiquinone, Q_8, which is the natural redox partner of Pox in the present case, and lipid (DMPC) molecules were first loaded by fusion of mixed lipid/Q_8 vesicles. The amount of Q_8 was given by the cyclic voltammogram recorded in a buffer solution at potential scan rate (v) slow enough to ensure that the total amount n_Q^0 of available Q_8 molecules introduced within the bilayer could reach the bottom of the pore by lateral diffusion and be reduced at the electrode surface. At $v \leq 0.01$ V/s, integration of the reduction peak gives n_Q^0 of $(30 \pm 3) \times 10^{-12}$ mole. The bilayer surface area of the microporous structure being 4.7 cm^2, the total amount of quinone within the bilayer corresponds to a Q_8/lipid molar ratio of 1.4% and to a surface concentration $\Gamma_Q^0 = (6.8 \pm 2) \times 10^{-12}$ mol cm^{-2}. The cyclic voltammogram of Q_8 (dotted line) shown in Figure 2 gives the typical behavior of such a quinone pool at a scan rate of 0.01 V/s in the presence of phosphate buffer.

Pyruvate oxidase was loaded as follows. The microporous electrode was dipped 10 min in the enzyme solution (36 μg/cm^3) in the presence of substrate and cofactor (pyruvate 10^{-2} M, Mg^{2+} 2×10^{-2} M, TPP 2×10^{-4} M) the enzyme exposing then its membrane binding site and being able to interact with the supported layer (as POx in Figure 1). After rapid rinsing in the same solution (without POx), the cyclic voltammogram exhibited a typical catalytic shape (*24*) in the presence of pyruvate (Figure 2, continuous line). The increase in current observed at potentials positive enough to oxidize the reduced form of Q_8 reflects the regeneration of the reduced ubiquinone by the enzyme catalyzed oxidation of pyruvate. It is worth underlining that no water-soluble mediator is present. Thus the catalytic current results from the following catalytic cycle:

step 1: $POx + pyruvate \rightarrow POx_{reduced} + acetate + CO_2$

step 2: lateral diffusion of Q_8 within the bilayer

step 3: $POx_{reduced} + Q_8 \rightarrow POx + Q_8H_2$

step 4: lateral diffusion of Q_8H_2 within the bilayer

step 5: $Q_8H_2 \rightarrow Q_8 + 2H^+ + 2e$
hence the flow of an anodic current

Steps 2, 3, and 4 take place within two dimensions, step 3 being the most interesting since the electrons (and protons) are transferred between the peripheral enzyme, anchored in the bilayer, and the ubiquinone, which is located solely within the bilayer. Step 3 mimics the physiological behavior of the enzyme and the catalytic current measures both the incorporation of the enzyme and its catalytic activity when anchored in the two-dimension structure.

The catalytic current of Figure 2 was found to decrease each time the potential scan was repeated. That suggested that either the enzyme was inactivated during the catalytic cycle or the peripheral protein was leaking from the supported layer. A systematic study of the enzyme incorporation was then examined.

Study of the Enzyme Incorporation in the Supported Layer. In general, successful incorporation of peripheral proteins in model bilayers such as proteoliposomes is ascertained by the recovery of the protein functionality. For example,

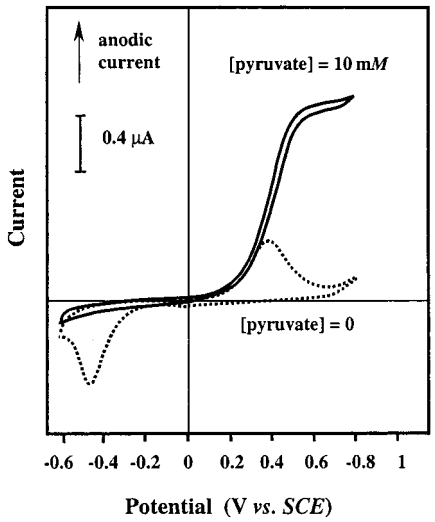

FIGURE 2: Cyclic voltammetry of the ubiquinone pool (Q_8) in the presence of pyruvate oxidase bound to the supported mimetic bilayer. Potential scan rate: 0.01 V/s. Dotted line: voltammogram without enzyme activity, at pyruvate concentration = 0 or before the POx loading. Continuous line: in the presence of catalytic coupling due to enzyme activity, pyruvate concentration = 10^{-2} M, POx assembled at 36 μg/cm^3. Background composition: 0.1 M, pH 6, phosphate buffer, 2×10^{-4} M TPP, 2×10^{-2} M Mg^{2+}. Temperature: 35 °C. Argon atmosphere. The microporous electrode was loaded with $(30 \pm 3) \times 10^{-12}$ mol of Q_8.

incorporation of microsomal cytochrome b_5 in proteoliposomes containing cytochrome P450 was attested by the reduction of cytochrome b_5 (*26*), or the reconstitution of pyruvate oxidase in a minimal respiratory chain was proved by its catalytic coupling with a terminal oxidase through a quinone pool (*15*).

We proceed similarly since the catalytic current is a measure of the two-dimension coupling between the enzyme catalysis and the electrochemical reaction through the quinone pool. However, we also monitored the incorporation of POx in a similarly supported bilayer by means of surface plasmon resonance (SPR) analysis. Alkylated sensor chips (HPA chips for Biacore from Pharmacia) are now commercially available for the SPR measurement of protein interactions with a supported lipid layer (*27*). Then, the alkylated layer is made of self-assembled octadecyl thiol (OM) at a flat gold surface. This first hydrophobic layer is very similar to the OTS layer covering the oxide in our microporous device. The properties of the upper lipid layer produced in both cases by fusion of lipid vesicles should be very similar. For example, the area occupied by a lipid molecule was very close in both cases: RPS analysis on HPA sensor chips gives 64 $Å^2$/lipid molecule (*27*) as compared to an area of 67 $Å^2$/lipid molecule which was measured by radioactive labeling in the microporous structure (*6*).

Figure 3 shows a qualitative comparison of enzyme incorporation in the supported layers through the two experimental approaches. In the first case, SPR analysis was used to follow the amount of proteins bound to the surface. After lipid loading of the HPA chip surface by fusion of vesicles (not shown), part A gives typical kinetics of association and dissociation between the enzyme and the layer. As soon as the POx solution is injected in its reduced form (in the presence of pyruvate and cofactors), the POx molecules interact with the membrane and accumulate. The

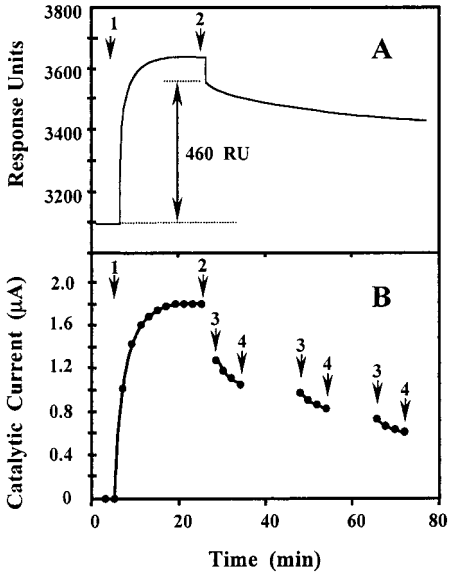

FIGURE 3: Kinetics of association and dissociation between pyruvate oxidase and the supported lipid layer. Comparison between two independent experiments. (A) Experimental trace of the SPR response on the Biacore apparatus. Arrow 1: introduction of the POx + pyruvate solution on the HPA chip formerly loaded with a lipid monolayer. Arrow 2: rinsing by injection of the pyruvate solution without POx. (B) Catalytic plateau currents sampled at 0.8 V during continuous cycling voltammetry (cycling between −0.7 V to 0.8 V/SCE at a potential scan rate of 0.1 V/s). The microporous electrode was formerly loaded with a lipid monolayer. Arrow 1: introduction of POx under the same conditions as in panel A. Arrow 2: pause of the voltammetric measurement, rinsing of electrode and cell with the pyruvate solution. Periods beginning at arrows 3 and ending at arrows 4: continuous cycling in the pyruvate solution. Arrows 4 to arrows 3: pause of the voltammetric excitation, the electrode staying in the same pyruvate solution. The complete electrochemical experiment was repeated after new dipping of the electrode for 80 min in the POx solution and gave the same results. Composition of the deaerated solution: 25 μg/cm^3 POx in 0.1 M, pH 6, phosphate buffer, 2×10^{-4} M TPP, 2×10^{-2} M Mg^{2+} and 0.05 M pyruvate.

signal is given in arbitrary response units (RU) and the SPR measurement of the bound enzyme can be determined, provided that the signal due to the protein in solution be deduced. For this experiment we found about 460 RU of bound protein. Rinsing shows that the incorporation of the protein is reversible. Such a reversibility was apparently not reported previously in the literature, certainly because as discussed later on, the proteoliposomes were studied in the presence of POx in all cases. However, the reversibility was implicitly expected (*2*) since the relation between enzyme activation and lipid binding plays an essential role in the physiological function of the enzyme in vivo (*19*).

Panel B of Figure 3 shows that similar kinetics of association and dissociation between the active enzyme and the model bilayer are observed by the electrochemical approach. The catalytic current increases at a rate close to the one appearing in panel A. That demonstrates that only the enzymes associated with the model bilayer are activated and kinetically coupled with the quinone pool. As expected, the soluble form of the enzyme, although rapidly introduced in the solution at the time of arrow 1, cannot exchange electrons with the ubiquinone partner confined within the bilayer. This is coherent with the fact that enzyme activation by lipid binding results from conformational changes in the environment of the bound flavin, making it more accessible to the electron-transfer reaction (*28*). Two types of dissociation kinetics can be observed then. Dissociation in the rinsing solution proceeds rather fast between arrows 3 and 4 and at a much slower rate, which is similar to the rate recorded in panel A between arrows 4 and 3. Between arrows 3 and 4, the potential is cycled continuously. Consequently, the enzyme redox state is caused to oscillate between the oxidized and the reduced forms. The main reason for the loss is the leakage of the oxidized form of POx which interacts weakly with the lipids (*19*). In contrast, the enzyme exists only in its reduced form during the periods separating arrows 4 and 3, and leakage results from simple dissociation of the reduced enzyme as occurs in panel A.

An estimation of the mass of protein retained per unit of the surface area can be derived from the SPR measurement (*29*, *30*). Using the calibration curve of Stenberg et al. (*29*) or the calculations of Sigal et al. (*30*), the 460 RU of Figure 3 correspond to ca. 50 ng/cm^2. Unfortunately, despite various attempts in a large range of protein concentration (from 5 to 100 μg/cm^3), we never succeeded in controlling specific and/or nonspecific binding of the proteins contained in our POx sample to the lipid/HPA structure. For example, in a series of 12 experiments at 36 μg/cm^3, the mass of bound protein was found to lie between 40 and 90 ng/cm^2. It seems that the poor reproducibility was a consequence of either small changes in the binding capacity of the HPA supported lipid layers and/or of nonspecific binding of the non-flavoprotein impurities contained in the POx sample. On the other hand, the catalytic current was solely proportional to the amount of incorporated enzyme that was active, and its reproducibility was quite good.

Quantitative Characterization of Pyruvate Oxidase Catalysis. When the redox partner of the enzyme is electroactive, it has been proven that cyclic voltammetry can be used quite efficiently to investigate the kinetics of water-soluble oxidoreductases. The required theoretical approaches were developed and extended (*31*−*33*). Similar studies were performed when the electron carrier was included in micelles (*34*) or when the enzymes were immobilized (*25*). Such models of heterogeneous enzymology are adapted here to the specific problem of membrane enzymes exchanging electrons with a redox partner like isoprenic quinones that are soluble in the bilayer only.

The experimental stability of the catalytic currents recorded with microporous electrodes shows that a stable incorporation of active POx can be obtained, provided that equilibrium with enzyme in solution is maintained. At constant surface concentration of POx, the measured current results from the electrocatalytic cycle described that combines three types of kinetic processes: (i) enzymatic catalysis by POx molecules embedded in the bilayer, (ii) two-dimension diffusion of ubiquinone and ubiquinol molecules within the bilayer, and (iii) electrochemical reaction of the ubiquinone/ubiquinol couple at the electrode/bilayer contact.

The POx enzyme released from *E. coli* is a homotetramer with a subunit of ca. 60 000 molar weight. Each subunit contains one tightly bound, although noncovalently, FAD and requires addition of one TPP + Mg^{2+} cofactor for the expression of its catalytic activity. The dissociation constant (K_d) of the enzyme−TPP complex has been shown to be very small. For the lipid activated POx species, K_d is ca. 3

μM (*35*). Therefore, in the presence of the TPP concentration used in the electrochemical experiments we carried out, the enzyme can be taken as existing permanently in its TPP complex form which will be noted E-FAD or E-$FADH_2$ in the following, E-FAD and E-$FADH_2$ being the oxidized and the reduced active enzymes, respectively. In the following, we will also consider that the surface concentration in active enzyme Γ_E is the active flavin surface concentration assuming each subunit of the activated tetramer exhibits the same activity (*20*).

Among the numerous reports concerning the activation of POx by amphiphiles, only a few dealt with the catalytic mechanism (*17*, *18*, *36*). The mechanistic studies were carried out in pseudohomogeneous solutions (solutions of micelles), and, most often, the artificial electron acceptor was ferricyanide. However, after reconstitution of purified POx in proteoliposomes, it was also established that Q_8 is physiologically the primary electron acceptor (*15*, *37*).

At physiological pyruvate concentrations, with ferricyanide as the redox partner, it was shown that the amphiphile activated POx catalysis proceeds according to a ping-pong mechanism with enzyme cycled between the oxidized and the reduced states (*17*, *18*). At pyruvate concentrations greater than 100 mM, which have no physiological significance, the kinetic signature of the mechanism becomes less clear (*18*). With Q_8 as the redox partner, we assume that the simple ping-pong mechanism consisting of the three following steps can be used to carry out the quantitative analysis of the observed kinetics.

$$\text{E-FAD} + \text{pyruvate} \underset{k_{-1}}{\overset{k_1}{\rightleftharpoons}} \text{E-FAD,pyruvate}$$

$$\text{E-FAD,pyruvate} \xrightarrow{k_2} \text{E-FADH}_2 + \text{acetate} + \text{CO}_2$$

$$\text{E-FADH}_2 + \text{Q}_8 \xrightarrow{k_3} \text{E-FAD} + \text{Q}_8\text{H}_2$$

Then, at any time t and at the enzyme active site located on the lipid layer at distance x from the electrode surface, the rate of consumption of Q_8 by the enzyme catalyzed reaction is related to the ubiquinone surface concentration Γ_Q by (*33*):

$$\left(-\frac{\partial \Gamma_Q}{\partial t}\right)_E = \frac{k_3\,\Gamma_E^0\,\Gamma_Q}{1 + k_3\Gamma_Q[1/k_2 + 1/(k_{red}\,C_P^0)]}$$

with Γ_E^0 and C_P^0 the enzyme surface concentration (mol/cm^2) and pyruvate bulk volume concentration (mol/cm^3), respectively, and with $k_{red} = k_1k_2/(k_{-1} + k_2)$. Thus, k_2, k_3, and k_{red} are expressed in s^{-1}, mol^{-1} cm^2 s^{-1} and mol^{-1} cm^3 s^{-1}, respectively.

Diffusion of pyruvate in solution proceeds certainly fast enough, as compared to its enzyme consumption at the lipid layer surface, to ensure that pyruvate concentration at the enzyme active site is practically equal to the pyruvate bulk concentration C_P^0.

The ubiquinone electron carrier is brought to the enzyme by lateral diffusion within the supported lipid bilayer (*5*−*8*) whose rate is given by the second Fick law:

$$\left(\frac{\partial \Gamma_Q}{\partial t}\right)_{diff} = D\,\frac{\partial^2 \Gamma_Q}{\partial x^2}$$

with D (cm^2/s) the lateral diffusion coefficient of both the oxidized and the reduced forms of ubiquinone within the supported lipid bilayer.

The oxidized form Q_8 of the electron carrier is regenerated at the electrode surface according to step 5, and the resulting flux of Q_8 leaving the electrode is given by a conveniently modified version of the Butler−Volmer equation (*7*, *38*):

$$-D\left(\frac{\partial \Gamma_Q}{\partial x}\right)_0 = k_0\left\{[\Gamma_Q^0 - (\Gamma_Q)_0]\exp\left[\frac{2\times 0.25F}{RT}(E - E_{pH}^{0'})\right] - (\Gamma_Q)_0\exp\left[\frac{2\times 0.75F}{RT}(E - E_{pH}^{0'})\right]\right\}$$

with F the Faraday constant, E the electrode potential, k_0 (cm/s) the rate constant of step 5 at the apparent standard potential $E_{pH}^{0'}$ of the Q_8H_2/Q_8 redox couple at pH of the buffered experiment, Γ_Q^0 the total surface concentration of electron carrier in both its reduced and oxidized forms (Q_8H_2 + Q_8), and $(\Gamma_Q)_0$ the concentration of the oxidized form at $x = 0$. The time dependence of the electrode potential is given by $E = E_i + \upsilon t$, with E_i the starting potential and υ the potential scan rate. The starting potential E_i is chosen so that all the electron carrier exists in its reduced form (Q_8H_2) at equilibrium when the working gold electrode potential is held at E_i.

As in the first Fick law, the current i can also be related to the concentration vs x profile:

$$i = -2FD(n_Q^0/l)(\partial q/\partial x)_{x=0}$$

with q the dimensionless concentration defined as Γ_Q/Γ_Q^0, l the length of the bilayer perpendicular to the electrode (the length of the pores), and n_Q^0 the total number of moles of electron carrier determined at potential scan rates slow enough ($\upsilon \leq 0.01$ V/s) to ensure that all of Q_8H_2 is oxidized into Q_8. Then the current recorded at the end of the forward potential scan must fall down to its background value.

The values of $E_{pH}^{0'} = -0.12$V/SCE (*8*) and $l = 4.5 \times 10^{-4}$ cm are known. The diffusion coefficient of Q_8 ($D = 3.8 \times 10^{-8}$ cm^2/s) measured by chronocoulometry as previously described (*7*) was found unchanged after POx loading. In the absence of pyruvate, the potential at which a peak appears in the voltammogram (see Figure 4) depends solely on the dimensionless parameter $\Lambda = k_0\sqrt{RT/2F\nu D}$ (see the Appendix). The best fit between simulation and experiment gives $k_0 = 5 \times 10^{-9}$ cm/s. The experimental peak height gives the proportionality coefficient of 2.18 μA relating the experimental peak height to Ψ_p, the computed dimensionless peak current, in agreement with the already mentioned values of D, n_Q^0, and l.

In the general case, once Λ is known, the current depends on both dimensionless parameters $\lambda = k_3\Gamma_E^0(RT/2F\nu)$ and $\sigma = k_3\Gamma_Q^0[1/k_2 + 1/(k_{red}\,C_P^0]$ when the catalysis is operating, as explained in the Appendix.

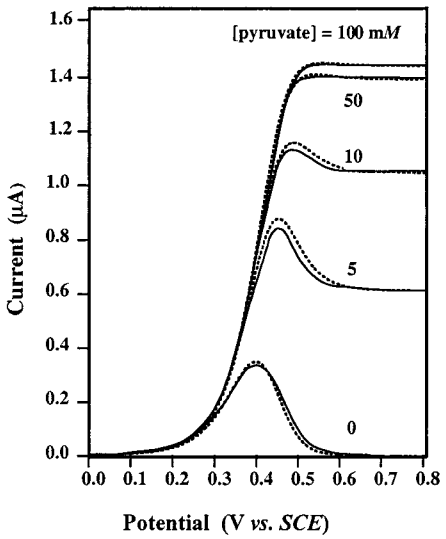

FIGURE 4: Voltammetry of the catalytic process, dependence of the voltammograms on pyruvate bulk concentration, the number on each curve gives the corresponding $C_P^0 = 0$ to 100 mM. The continuous curves are the experimental ones after correction for background current. The dotted curves are computed as described in the text for $\Lambda = 3 \times 10^{-5}$ and $\lambda = 2.25$, the relationship between σ and C_P^0 being as in Figure 5. $n_Q^0 = (30 \pm 3) \times 10^{-12}$ mol, $l = 4.5 \times 10^{-4}$ cm, $D = 3.8 \times 10^{-8}$ cm^2/s, area of the bilayer = 4.7 cm^2, same background solution as in Figure 2. Potential scan rate $v =$ 0.01 V/s. Temperature: 35 °C.

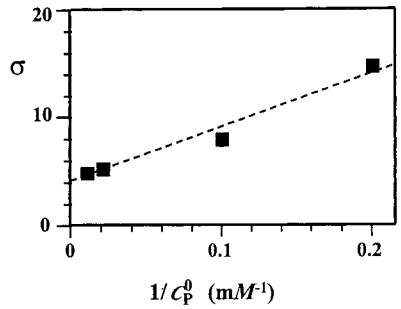

FIGURE 5: Voltammetry of the catalytic process, dependence of the dimensionless parameter σ (see text) on pyruvate bulk concentration C_P^0. The dotted line gives the best linear fit. Same experimental conditions as in Figure 4.

The dependence on σ is insignificant as long as q is small enough to ensure that $\sigma q \ll 1$. The latter condition may be fulfilled when the electrode potential is small enough. In the presence of bulk pyruvate concentrations $C_P^0 \geq 10$ mM, the experimental voltammograms reproduced in Figure 4 clearly show that the same currents are obtained whatever C_P^0 provided that $E \leq 0.35$ V/SCE. In such circumstances, the voltammogram depends solely on λ. The best fit between the experimental and the computed curves is obtained for $\lambda = 2.25 \pm 0.35$, meaning that $k_3\Gamma_E^0 = 1.70 \pm 0.25$ s^{-1}.

Once λ is known, the second parameter σ can be adjusted so as to obtain, at each C_P^0, the best fit between the experimental and the computed voltammograms over the whole range of explored potentials. The resulting σ versus $1/C_P^0$ plot is reproduced in Figure 5. The linearity of the plot supports the relevancy of the ping-pong mechanism. From the slope and intercept of the σ vs $1/C_P^0$ plot, we can deduce the Michaelis constant vs pyruvate $K_{MP} = k_2/k_{red} = 13 \pm 2$ mM and $k_3\Gamma_E^0/k_2 = 4.0 \pm 0.5$. The Michaelis constant vs Q_8 is $K_{MQ8} = k_2/k_3 = (1.8 \pm 0.7) \times 10^{-12}$ mol/cm^2 since $\Gamma_Q^0 = (6.8 \pm 2) \times 10^{-12}$ mol/cm^2 as already mentioned. Within experimental uncertainty, identical results were obtained when Γ_Q^0 was decreased down to 1.3×10^{-12} mol/cm^2.

The direct determination of k_3 would require an independent determination of Γ_E^0. As already mentioned, SPR measurements can give, at best, the total amount of proteins bound to the lipid layer, not the amount of active POx. A spectrophotometric determination of the enzymatically active flavin cannot be performed, the amount of flavin being much too small to be detectable. The rate constant in two dimensions k_3 can be estimated as follows. It seems reasonable to assume that the pyruvate related turnover of POx (k_2 in s^{-1}), which equals the turnover related to a bielectronic electron acceptor or is twice the turnover related to a monoelectronic electron acceptor, is similar in the present case to the those reported in previous studies. In most cases, POx activities have been measured in the presence of saturating pyruvate, TPP, and electron acceptor concentrations. Under such conditions, k_2 could be determined directly. The values we found in the literature range from 105 s^{-1}, with Q_8 as the electron acceptor and POx located in *E. coli* membrane vesicles (*15*), to 180 ± 10 s^{-1}, with ferricyanide as the electron acceptor and POx in SDS micelles (*18*). If we assume that $k_2 = 150 \pm 40$ s^{-1}, we obtain $k_3 = (1.1 \pm 0.6) \times 10^{14}$ mol^{-1} cm^2 s^{-1} and $\Gamma_E^0 = (2.4 \pm 1.5) \times 10^{-14}$ mol/cm^2.

If the 40−90 ng/cm^2 of proteins retained on the lipid layer in the SPR experiments were made solely of active POx subunits of 60000 g molar weight, Γ_E^0 would be ca. 10^{-12} mol/cm^2. The comparison shows clearly that most of the proteins bound to the lipid layer are not catalytically active. The fact that the Q_8 diffusion coefficient was not affected by protein incorporation indicates also that few proteins are really embedded in the bilayer and able to alter the lateral mobility by archipelago effect.

The reactivity of the reduced enzyme with Q_8 is expressed by rate constant k_3. Its value is at least 3 orders of magnitude below the limit corresponding to a diffusion-controlled reaction in two dimensions (*3*, *39*). Owing to the originality of the determination of k_3 in two dimensions, there are no data available in the literature to which we could compare the significance of the value we found.

The fact that we find a K_{MP} value in agreement with those reported earlier in the literature (see the Table) also confirms the adequacy of the ping-pong mechanism since, according to such a mechanism, the kinetics of reduction of the oxidized enzyme by pyruvate substrate does not depend on the nature of redox partner, be it Q_8 or ferricyanide as in ref *18*.

Determined Value of K_{MQ8} versus Ubiquinone Concentrations in Physiological Membranes. To our knowledge, it is the first time a Michaelis constant K_{MQ8} is determined for an electron exchange reaction in two dimensions. Its knowledge gives access to the quantitative analysis of membrane bound enzyme kinetics in a way that takes actually into account the restriction of the freedom of motion of the quinone electron carrier to two dimensions only.

The ubiquinone content (Q_7 to Q_{10}) in systems of electron transport along membranes is 0.5−2% of the lipid content (*41*−*43*). That corresponds to ubiquinone surface concentrations Γ_Q^0 of (2.5 to 10) $\times 10^{-12}$ mol/cm^2, the lipid surface

Table 1: Kinetic Constants of Activated Pyruvate Oxidase[a]

Two Dimensions	
constants	this work
K_{MQ8}	$(1.8 \pm 0.7) \times 10^{-12}$ mol/cm^2
k_3[b]	$(1.1 \pm 0.6) \times 10^{14}$ mol^{-1} cm^2 s^{-1}

Three Dimensions		
constants	this work	literature
K_{MP}	$(13 \pm 2) \times 10^{-3}$ mol/L[c]	$7-25 \times 10^{-3}$ mol/L[d,e]
k_2[f]	taken as 150 ± 40 s^{-1}	105[g] to 170−190[e,h,i] s^{-1}
K_{MQ1}	nd	2×10^{-4} mol/L[j]
$K_{M,ferri}$	nd	3×10^{-3} mol/L[e,i]

[a] Amphiphile-activated enzyme at 25 (literature) or 35 °C (this work), pH 6. [b] With the assumption that k_2 is as mentioned below. [c] Q_8 as electron acceptor. [d] From ref *16*, DCPIP as electron acceptor, and from ref 21, ferrocene methanol as electron acceptor. [e] From ref *18*, ferricyanide as electron acceptor. The kinetic constants are calculated from the initial velocities measured at pyruvate concentrations lower than 50 mM, assuming a ping-pong mechanism. [f] Flavin turnover per flavoprotein subunit, or quinone turnover, or half the ferricyanide turnover. [g] From ref *15*, with Q_8 in reconstituted *E. coli* membrane vesicles. [h] From ref *15*, a ferricyanide assay with Q_8 as primary electron acceptor. [i] From ref *40*. [j] From ref *15*, Q_1 as electron acceptor.

concentration being ca. 500×10^{-12} mol/cm^2. In particular, *E. coli* synthesizes ubiquinone-8 (Q_8) and menaquinone-8 in various proportions depending on growth conditions. Under strict anaerobic conditions, the culture contains 0.25×10^{-9} mol of menaquinone/mg of bacterial dry weight and no detectable amount of ubiquinone, whereas, under high aeration, 0.55×10^{-9} mol of Q_8/mg of bacterial dry weight are produced (*44*). This correlates with the fact that menaquinone is a very poor electron carrier for POx (*15*) and that POx feeds electrons in the aerobic respiratory chain. The amount of lipids in the cytoplasm membrane being 75% of the 0.091 mg of lipid/mg of bacterial dry weight (*45*), the Q_8 to lipid ratio is ca. 0.6 mol %. Neglecting the membrane surface area occupied by transmembrane proteins which is inaccessible to Q_8, that gives a physiological ubiquinone surface concentration Γ^0_Q of ca. 3×10^{-12} mol/cm^2 close to the ubiquinone content of 2.8×10^{-12} mol/cm^2, calculated by Hackenbrock et al. (*1*) or 2×10^{-12} mol/cm^2 measured by Wallace and Young (*46*). The K_{MQ8} of $(1.8 \pm 0.7) \times 10^{-12}$ mol/cm^2 that we determined in the present study is in the right range for the optimal exchanges of redox equivalents between POx and terminal oxidases via the quinone pool. When embedded in the bilayer, the enzyme would be efficiently regulated by the stationary ratio Q_8/Q_8H_2, that is to say by the oxidation level of the quinone pool.

CONCLUSION

It has been theoretically pointed out that the reduction of dimensionality may be advantageous for the efficiency of membrane-bound enzymes (*1*, *3*, *47*). It is also well established that isoprenic quinones are essential carriers that allow communication between enzyme complexes in most of electron transport chains taking place in physiological membranes (*1*, *15*, *48*). However there are few experimental means of quantitative investigation of the kinetic couplings that are involved then and that take into account the fact that these kinetic couplings must operate necessarily in two dimensions.

In the present study, we showed that the experimental limitations that are most often put forward can be overcome (*15*, *49*). We characterized quantitatively the kinetic steps that are required to proceed in two dimensions when the oxidation of pyruvate is catalyzed by pyruvate oxidase, a reasonably simple model of membrane bound enzyme. We used a relatively easy to handle lipid structure that was shown to mimic correctly the behavior of real membranes as far as the lateral mobility of the isoprenic quinone is concerned. The kinetic coupling of the enzyme bound to the lipid structure with the ubiquinone pool was ensured by the regeneration of the oxidized form of the quinone at an electrochemical interface.

ACKNOWLEDGMENT

We are grateful to Drs. Bertagnolli and Hager (University of Illinois, Champaign-Urbana) for the gift of *E. coli* mutant YYC458. Q_8 was a gift from EISAI Company LTD, Tokyo.

APPENDIX

Dimensionless Expression of the Equations Required for the Computation of the Cyclic Voltammogram. Introducing the dimensionless space variable $y = x\sqrt{2F\nu/RTD}$, the current i is given by:

$$i = 2F(n^0_Q/l)\sqrt{2F\nu D/RT\Psi}$$

with $\Psi = -(\partial q/\partial y)_{y=0}$ the dimensionless current.

Therefore numerical solution of the following set of equations gives Ψ hence i at any time, i.e., at any potential E, along the voltammogram (*50*, *51*).

$$\frac{\partial q}{\partial \tau} = \frac{\partial^2 q}{\partial y^2} - \frac{\lambda q}{1+\sigma q}$$

$$\Psi = \Lambda \exp(0.25\xi)\{1 - q_0[1 + \exp(-\xi)]\}$$

The following initial and boundary conditions must be taken into account: (i) at $\tau = 0$ and $y \geq 0$, $E = E_i$ and $q = 0$, (ii) at $\tau = 0$ and $y = 0$, $E = E_i$ and $q = 0$, (iii) at $y = h = l\sqrt{2F\nu/RTD}$ and $\tau \geq 0$, $-(\partial q/\partial y)_{y=h} = \lambda q_h/(1 + \sigma q_h)$, $\tau = t(2F\nu/RT)$ being the dimensionless time, q_0 and q_h the dimensionless concentrations at $y = 0$ and $y = h$, respectively, and $\xi = (2F/RT)(E - E^{0'}_{pH})$ the dimensionless potential.

The other dimensionless parameters are defined as:

$$\Lambda = k_0\sqrt{RT/2F\nu D}$$

$$\lambda = k_3\,\Gamma^0_E(RT/2F\nu)$$

$$\sigma = k_3\,\Gamma^0_Q[1/k_2 + 1/(k_{red}C^0_p)]$$

REFERENCES

1. Hackenbrock, C. R., Chazotte, B., and Gupte, S. S. (1986) *J. Bioenerg. Biomembr. 18*, 331−368.
2. Gennis, R. B. (1989) in *Biomembranes, Molecular Structure and Function*, Springer-Verlag, New York.
3. Adam, G., and Delbrück, M. (1968) in *Structural Chemistry and Molecular Biology* (Rich, A., Davidson, N., Eds) pp 198−215, Freeman, San Francisco.

4. Gelb, M. H., Jain, M. K., Hanel, A. M., and Berg, O. G. (1995) *Annu. Rev. Biochem. 64*, 653−688.
5. Torchut, E., Laval, J. M., Bourdillon, C., and Majda, M. (1994) *Biophys. J. 66*, 753−762.
6. Marchal, D., Boireau, W., Laval, J. M., Moiroux, J., and Bourdillon, C. (1997) *Biophys. J. 72*, 2679−2688.
7. Marchal, D., Boireau, W., Laval, J. M., Moiroux, J., and Bourdillon, C. (1998) *Biophys. J. 74*, 1937−1948.
8. Marchal, D., Boireau, W., Laval, J. M., Bourdillon, C., and Moiroux, J. (1998) *J. Electroanal. Chem. 451*, 139−144.
9. Masuda, H., and Fukuda, K. (1995) *Science*, *268*, 1466−1468.
10. Brian, A. A., and McConnell, H. M. (1984) *Proc. Natl. Acad. Sci. U.S.A. 81*, 6159−6163.
11. Plant, A. L. (1999) *Langmuir*, *15*, 5128−5135.
12. Tocanne, J.-F., Dupou-Cézanne, L., and Lopez, A. (1994) *Prog. Lipid Res. 3*, 203−237.
13. Sackmann, E. (1996) *Science*, *271*, 43−48.
14. Wong, J. Y., Majewski, J., Seitz, M., Park, C. K., Israelachvili, J. N., and Smith, G. S. (1999) *Biophys. J. 77*, 1445−1457 and 1457−1468.
15. Koland, J. G., Miller, M. J., and Gennis, R. B. (1984) *Biochemistry*, *23*, 445−453.
16. Cunningham, C. C., and Hager, L. P. (1971) *J. Biol. Chem. 246*, 1583−1589.
17. Bertagnolli, B. L., and Hager, L. P. (1991) *J. Biol. Chem. 266*, 10168−10173.
18. Mather, M., and Gennis, R. (1985) *J. Biol. Chem. 260*, 16148−16155.
19. Chang, Y. Y., and Cronan, J. E. (1984) *Proc. Natl. Acad. Sci. U.S.A. 81*, 4348−4352.
20. Wang, A., Chang, Y. Y., and Cronan, J. E. (1991) *J. Biol. Chem. 266*, 10959−10966.
21. Pierrat, O., Bourdillon, C., Moiroux, J., and Laval, J. M. (1998) *Langmuir*, *14*, 1692−1696.
22. Williams, F. R., and Hager, L. P. (1966) *Arch Biochem. Biophys. 116*, 168−176.
23. Miller, C. J., and Majda, M.**(**1986) *J. Am. Chem. Soc. 108*, 3118−3120.
24. Parpaleix, T., Laval, J. M., Majda, M., and Bourdillon, C. (1992) *Anal. Chem. 64*, 641−646.
25. Bourdillon, C., Demaille, C., Moiroux, J., and Savéant, J. M. (1996) *Acc. Chem. Res. 29*, 529−536.
26. Yamazaki, H., Johnson, W. W., Ueng, Y. F., Shimada, T., and Guengerich, F. P. (1996) *J. Biol. Chem. 271*, 27438−27444.
27. Cooper, M. A., Try, A. C., Carroll, J., Ellar, D. J., and Williams, D. H. (1998) *Biochim. Biophys. Acta 1373*, 101−111.
28. Mather, M., and Gennis, R. (1985) *J. Biol. Chem. 260*, 10395−10397.
29. Stenberg, E., Persson, B., Roos, H., and Urbaniczky, C. (1991) *J. Colloid Interface Sci. 143*, 513−526.
30. Sigal, G. B., Bamdad, C., Barberis, A., Strominger, J., and Whitesides, G. M. (1996) *Anal. Chem. 68*, 490−497.
31. Bourdillon, C., Bourgeois, J. P., and Thomas, D. (1980) *J. Am. Chem. Soc. 102*, 4231−4235.
32. Cass, A. E. G., Davis, G., Francis, G. D., Hill, H. A. O., Aston, W. J., Higgins, I. J., Plotkin, E. V., Scott, L. D., and Turner, A. F. P. (1984) *Anal. Chem. 56*, 667−675.
33. Bourdillon, C., Demaille, C., Moiroux, J., and Savéant, J. M. (1993) *J. Am. Chem. Soc. 115*, 2−10.
34. Deshaies, C., Chopineau, J., Moiroux, J., and Bourdillon, C. (1996) *J. Phys. Chem. 100*, 5063−5069.
35. O'Brien, T. A., Blake, R., and Gennis, R. B. (1977) *Biochemistry 16*, 3105−3109.
36. Houghton, R. L., and Swoboda, B. E. P. (1973) *Biochem. Soc. Trans. 1*, 665−667.
37. Carter, K., and Gennis, R. B. (1985) *J. Biol. Chem. 260*, 10986−10990.
38. Laviron, E. (1983) *J. Electroanal. Chem. 146*, 15−36.
39. Keizer, J. (1985) *Acc. Chem. Res. 18*, 235−241.
40. Blake, R., Hager, L. P., and Gennis, R. B. (1978) *J. Biol. Chem. 253*, 1963−1971.
41. Hauska, G., and Hurt, E. (1982) in *Function of Quinones in Energy Conserving Systems*, (Trumpower, B. L. Ed.), pp 87−124, Academic Press, New York.
42. Schneider, H., Lemasters, J. J., Hochli, M., and Hackenbrock, C. R. (1980) *J. Biol. Chem. 255*, 3748−3756.
43. Knoell, H. E. (1979) *Biochem. Biophys. Res. Commun. 91*, 919−925.
44. Ingledew, W. J., and Poole, R. K. (1984) *Microbiol. Rev. 48*, 222−271.
45. Neidhardt, F. C. (1984) in *Escherichia coli and Salmonella typhimurium, Cellular and Molecular Biology* (Neidhardt, F.C., Ed) Vol 1, pp 4, 32, American Society for Microbiology, Washington, D. C.
46. Wallace, B. J., and Young, I. G. (1977) *Biochim. Biophys. Acta* 461, 84−100.
47. Bücher, T. (1953) *Adv. Enzymol. 14*, 1−47.
48. Chazotte, B., and Hackenbrock, C. R. (1988) *J. Biol. Chem. 263*, 14359−14367.
49. Kröger, A., and Klingenberg, M. (1973) *Eur. J. Biochem. 39*, 313−323.
50. Smith, G. D. (1971) *Numerical Solutions of Partial Differential Equations*, p 23, Oxford Mathematical Handbook, London.
51. Bourdillon, C., Demaille, C., Moiroux, J., and Savéant, J. M. (1995) *J. Am. Chem. Soc. 117*, 11499−11506.

BI002325Y